Nano Research
2022, 15(10): 9447–9453

ISSN 1998-0124 CN 11-5974/O4
https://doi.org/10.1007/s12274-022-4520-2

Research Article

Chirally assembled plasmonic metamolecules from intrinsically chiral nanoparticles

Jiahao Pan[1,2], Xiaoyao Wang[1,2], Jinjin Zhang[2,3], Qin Zhang[2,4], Qiangbin Wang[1,2,5], and Chao Zhou[1,2] (✉)

[1] *School of Nano-Tech and Nano-Bionics, University of Science and Technology of China, Hefei 230026, China*
[2] *CAS Key Laboratory of Nano-Bio Interface, Suzhou Key Laboratory of Functional Molecular Imaging Technology, Division of Nanobiomedicine and i-lab, Suzhou Institute of Nano-Tech and Nano-Bionics, Chinese Academy of Sciences, Suzhou 215123, China*
[3] *Nano Science and Technology Institute, University of Science and Technology of China, Suzhou 215123, China*
[4] *Jiangsu Key Laboratory of Thin Films, School of Physical Science and Technology, Soochow University, Suzhou 215006, China*
[5] *College of Materials Sciences and Opto-Electronic Technology, University of Chinese Academy of Sciences, Beijing 100049, China*

Received: 22 April 2022 / **Revised:** 9 May 2022 / **Accepted:** 9 May 2022

ABSTRACT

Significant chiroptical responses could be generated by chiral coupling of achiral plasmonic nanoparticles, or originated from intrinsically chiral plasmonic nanoparticles. Here we create dimeric plasmonic metamolecules possessing both chiral coupling between nanoparticles and intrinsic chiroptical responses derived from nanoparticles themselves. These plasmonic metamolecules are prepared by assembling helical plasmonic nanorods (HPNRs) with intrinsic chirality in chiral manners on DNA origami template. Two HPNRs with the same or opposite chirality, or one HPNR and one achiral gold nanorod, are coupled chirally into dimeric metamolecules with intriguing plasmonic circular dichroism (PCD). We found that both of the intrinsic chirality of constituent HPNRs and the chiral coupling contribute to the overall PCD while their weights are different in different metamolecules and vary in different wavelength range for a certain metamolecule. Comparing to conventional chiral plasmonic metamolecules from achiral nanoparticles, or discrete chiral nanoparticles, these metamolecules bring more dimensions for tailoring chiroptical responses and make it more flexible to design plasmonic nanodevices with custom PCD.

KEYWORDS

chiral plasmonics, DNA origami, plasmonic circular dichroism, gold nanoparticle

1 Introduction

Plasmonic nanoparticles manifest strong interactions with light due to the phenomenon known as localized surface plasmon resonance, in which the free electrons of nanoparticles oscillate upon incident light of certain wavelength [1, 2]. Fabricating the size, shape and composition of plasmonic nanoparticle offers a feasible way to manipulate light and generate unique optical properties [3, 4]. Furthermore, organizing such nanoparticles with proximity into plasmonic metamolecules would give rise to new properties, e.g., plasmonic chirality [5–12]. In specific, arranging spherical gold nanoparticles or gold nanorods (AuNRs) in chiral manners would yield plasmonic metamolecules with chiroptical properties that isolated nanoparticles do not possess [13–15]. Among various strategies, DNA origami-based assembly is a particular way to build plasmonic metamolecules [16–18]. DNA origami is self-assembled based on precise sequence hybridization, which owns full addressability with nanoscale resolution and therefore could be employed as an ideal platform to locate nanoparticles [19, 20]. In the past decade, this strategy has achieved great success to create chiral plasmonic metamolecules from static to dynamic [21–30].

On the other hand, plasmonic chirality could be realized by fabricating nanoparticles with chiral shape [31–33]. Recently, controllable synthesis of chiral nanoparticles with intrinsic chiroptical responses became practical [34–42]. Like chiral metamolecules from achiral nanoparticles, these intrinsically chiral nanoparticles exhibit pronounced plasmonic circular dichroism (PCD). Furthermore, these chiral nanoparticles could be coupled by ligand-mediated assembly [38, 43–45]. While these two modes of developing plasmonic chirality are independent, here we create dimeric metamolecules which possess chiroptical responses both from the chiral shape of nanoparticles as well as the chiral coupling between nanoparticles. These plasmonic metamolecules are prepared by coupling intrinsically chiral nanoparticles in chiral manners employing DNA origami as the template. Either two nanoparticles with the same chirality or a pair of enantiomeric chiral nanoparticles could be coupled in controlled manner to form particular dimeric plasmonic metamolecules. We analyze their PCD and demonstrate that the overall chiroptical responsiveness consists of both the intrinsic chirality of nanoparticles and the plasma coupling guided by chiral assembly. This work provides a novel pathway to create chiral plasmonic metamolecules and makes it possible to custom chiroptical responses from both the building blocks as well as the coupling mode.

Address correspondence to czhou2018@sinano.ac.cn

2 Results and discussion

The most basic form of chiral plasmonic metamolecules is dimer of AuNR, in which each anisotropic nanoparticle can be a dipole and minimally two dipoles can form a chiral conformation [24, 46]. To follow this simplest strategy, we employed helical plasmonic nanorods (HPNRs) as building blocks for the dimeric metamolecules. The HPNRs have strong PCD due to their intrinsic chirality [37–39, 47]. Similar to ordinary AuNRs, their orientation could be well-controlled on DNA origami template, which is critical for creating metamolecules with expected conformations. The synthesis of HPNRs are adapted from a previous work [39]. In short, they were obtained by depositing reduced Au and Ag atoms on AuNRs modified by ligands of L- or D-cysteine and 4-aminothiophenol molecules. The as-synthesized HPNRs have the length of around 60 nm and diameter of around 20 nm, exhibiting a transverse resonance band at approximately 524 nm and longitudinal resonance band at around 790 nm respectively with similar intensity (Figs. 1(a), 1(c), and 1(d)). Their PCD spectra are determined by their intrinsic chirality, which are controlled by choosing ligands of L- or D-cysteine during synthesis. In the following, we use L-HPNRs (brown color in figures) and D-HPNRs (yellow color in figures) to denote these two HPNRs. The maximum *g*-factors of HPNRs we synthesized are approximately –0.013 for L-HPNRs and +0.013 for D-HPNRs at the transverse resonance band (Fig. 1(b)).

To assemble HPNRs on DNA origami, the HPNRs were firstly modified by thiolated DNA. Considering the rugged surface morphology of HPNRs, thiolated DNAs with 20-nt were used, whose length is relatively longer than that for modifying conventional AuNRs. Meanwhile, we utilized an optimized strategy combining salt-aging and freeze-facilitated methods to ensure the stability of DNA-modified HPNRs in the buffer of DNA origami (detailed procedure in method section). After modification, we examined their absorption spectra, PCD spectra and *g*-factor spectra in the buffer with 500 mM Na^+, it turned out that there was no obvious difference from their original spectra, confirming they were well-dispersed and stable after DNA modification.

We designed a rigid two-layer DNA origami (approximately 50 nm × 48 nm × 4 nm) as the template for guiding the assembly of HPNRs. Two lines of staple strands are extended from the origami for capturing one HPNR (details in the Electronic Supplementary Material (ESM)). Each capture strand contains a 12-nt segment for hybridizing with DNA grafted on HPNR. As aforementioned, two NRs are enough for the chiral assembly of metamolecules. We prepared two typical chiral conformations of NR dimer, both of which were formed by arranging two HPNRs in a non-coplanar manner, while one is orthogonal dimer overlapped at the ends and the other one is crossed dimer overlapped at the centers (Fig. 2). The combination of these two conformations with either L-HPNR or D-HPNR building blocks yields up to 12 kinds of chiral plasmonic metamolecules. The metamolecules were purified by agarose gel electrophoresis after annealing process (Fig. 2(c)) and characterized by transmission electron microscopy (TEM) to confirm the successful assembly (Fig. 2(d)), more TEM images in Fig. S3 the ESM).

We first assembled metamolecules from two HPNRs with the same intrinsic chirality. For metamolecules of L-HPNR (Figs. 3(a) and 3(b)), all four metamolecules, including orthogonal dimer and crossed dimer assembled in either left-handed or right-handed manner, exhibit PCD spectra with a trough at short wavelength (around 560 nm) and a peak at long wavelength (around 790 nm). This feature is roughly consistent with the PCD spectrum of discrete L-HPNR, suggesting the chiroptical responses of these metamolecules are dominated by their intrinsic chirality. While the trough positions are nearly the same with that of intrinsic PCD spectra of L-HPNR, the peak positions show obvious blue-shift for left-handed metamolecules and red-shift for right-handed metamolecules. We ascribe this to the coupling of two

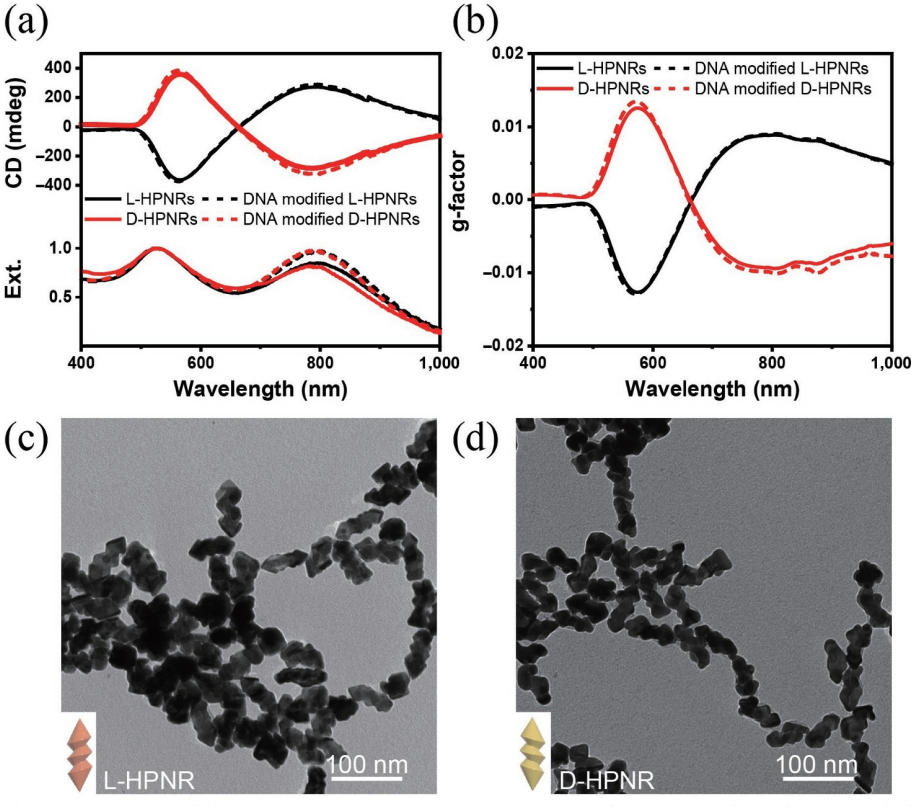

Figure 1 Plasmonic and chiroptical properties of the HPNRs. (a) PCD, UV–vis extinction and (b) *g*-factor spectra of L- and D-HPNRs before (solid curve) and after (dash curve) DNA modification; TEM images of (c) L-HPNRs and (d) D-HPNRs.

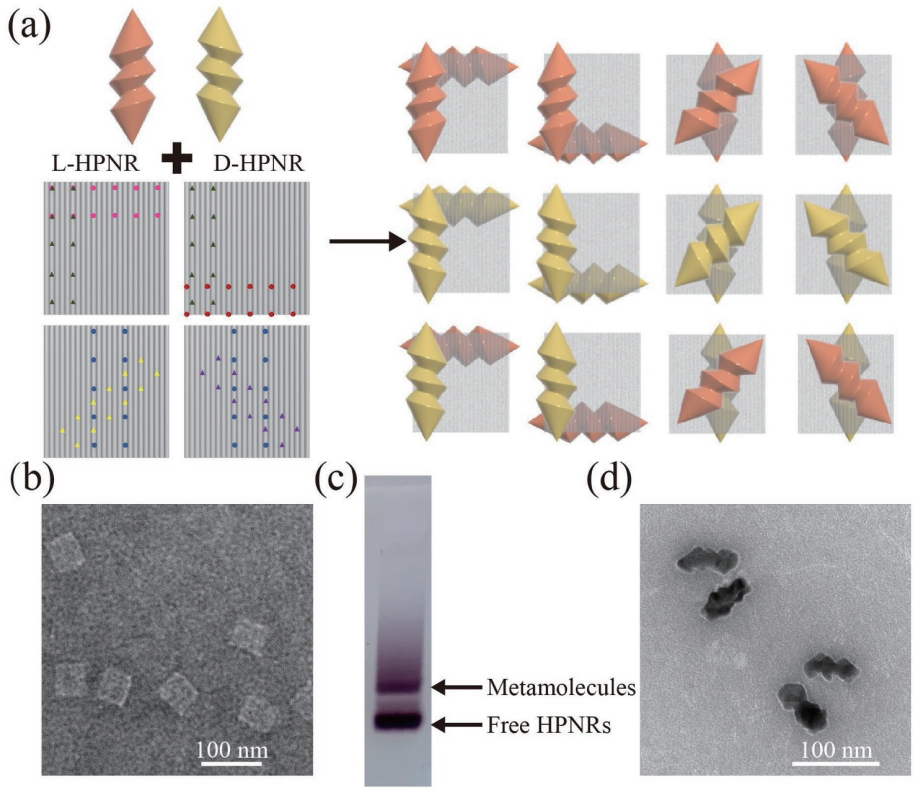

Figure 2 Fabrication of chiral HPNR metamolecules. (a) Schematic illustration for the assembly of 12 kinds of chiral plasmonic metamolecules. The triangle points represent the sites on the top layer and the circular points represent the sites on the bottom layer. (b) TEM image of the two-layer DNA origami. (c) Agarose gel electrophoresis and (d) representative TEM image of assembled chiral metamolecules (from metamolecules of right D-/L-HPNRs).

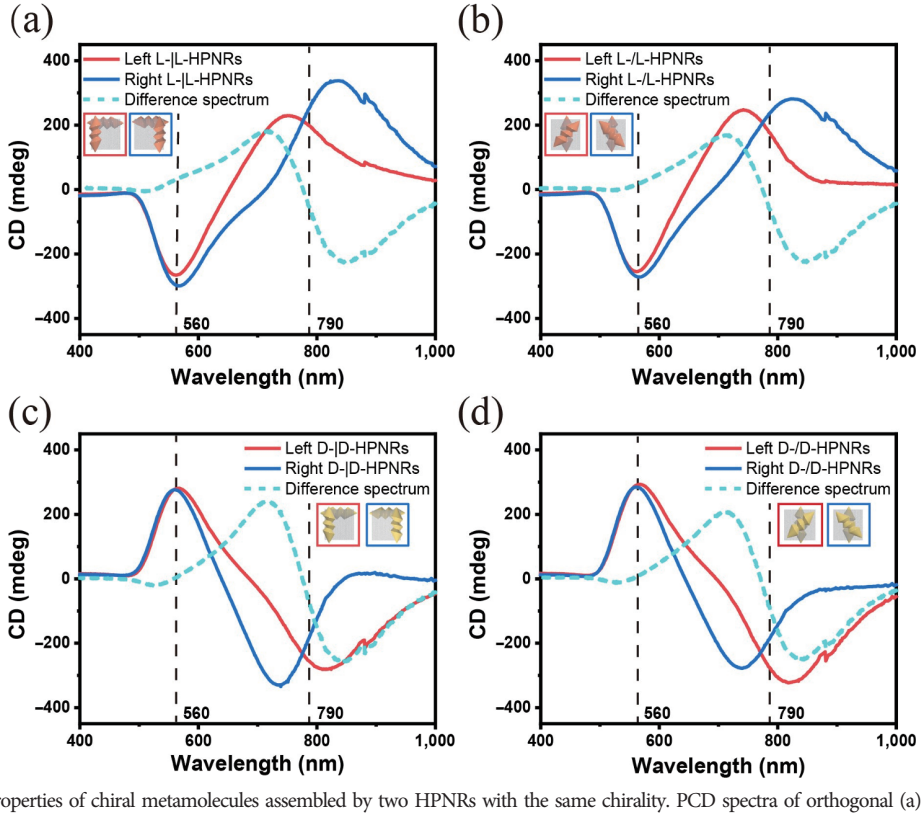

Figure 3 Chiroptical properties of chiral metamolecules assembled by two HPNRs with the same chirality. PCD spectra of orthogonal (a) and crossed (b) dimeric metamolecules assembled by two L-HPNRs as well as orthogonal (c) and crossed (d) dimeric metamolecules assembled by two L-HPNRs. In all four figures, the red curve denotes that of left-handed conformation and the blue curve denotes right-handed. The cyan dash curve refers to the difference spectrum respectively (left-handed minus right-handed). We name the metamolecules in this rule: The first left or right refers to their chiral conformation, and the next segment lists two constituent nanoparticles separated by "|" (orthogonal) or "/" (crossed); the same applies below.

nanoparticles in the longitudinal mode. To clearly show the contribution of chiral coupling, we calculated the difference spectra between the left-handed and right-handed metamolecules ($PCD_{left\text{-}handed} - PCD_{right\text{-}handed}$), which eliminate the part from their

intrinsic chirality (cyan dash curve in figures). For both orthogonal dimer and crossed dimer, the difference spectra are consistent with that of typical left-handed AuNR dimer metamolecules. As shown in Figs. 3(a) and 3(b), the bisignate difference spectra could be correlated to the longitudinal coupling of nanorods while the transverse coupling is much weaker. In addition, the difference spectra of subtracting PCD of constituent L- or D-HPNRs from PCD spectra of metamolecules are shown in Fig. S4 in the ESM.

For metamolecules assembled from D-HPNR, all the spectra show nearly mirrored shapes compared to their mirrored metamolecules (Figs. 3(c) and 3(d), and Fig. S4 in the ESM). It should be noted that a pair of mirrored metamolecules have mirrored conformation from assembly as well as mirrored intrinsic chirality from HPNRs. For example, the mirrored metamolecule of left-handed L-/L-HPNRs is right-handed R-/R-HPNRs, and their spectra are nearly mirrored (Fig. S4 in the ESM). In short, their PCD spectra are mainly determined by the intrinsic chirality of nanoparticles while the longitudinal coupling notably alters their chiroptical responses at long wavelength.

We then assembled metamolecules from two enantiomeric HPNRs. In specific, one L-HPNR and one D-HPNR are coupled to form one dimer. On one hand, such dimers could be regarded as a racemic mixture when disassembled. On the other hand, they could be assembled to form left- or right-handed conformations on the DNA origami template. To prepare these dimers, the L-HPNRs and D-HPNRs were modified by thiolated DNAs with different sequences. By extending corresponding capture strands from DNA origami template, L-HPNR was located at one surface and D-HPNR was at the other surface, ensuring all dimers were formed by two mirrored HPNRs. The PCD spectra of these metamolecules consisting of two enantiomeric HPNRs exhibit clear difference from dimeric metamolecules of AuNRs with the same conformations. As shown in Fig. 4, besides the strong longitudinal coupling, their PCD spectra show obvious transverse coupling at a short wavelength range. We speculate that the strong transverse coupling is related to the helical morphology at the side of nanorods. To confirm these features are induced by the coupling of HPNRs instead of their intrinsic properties, we disassembled these dimers by heating the samples to 65 °C and subsequently measured their PCD spectra. It turns out there is no obvious PCD responses at the whole wavelength range, suggesting the samples could be regarded as racemic mixtures when disassembled.

We further assembled dimeric metamolecules by coupling one HPNR with one conventional AuNR. We synthesized AuNRs with a similar length and diameter to the HPNR to build the metamolecules (Fig. S5 in the ESM). The TEM images of dimeric metamolecules demonstrate the successful assembly (Fig. 5(b), more TEM images in Fig. S7 in the ESM). We prepared eight metamolecules formed by one AuNR and either L- or D-HPNR and measured their PCD spectra, as shown in Figs. 5(c)–5(f). We also measured their PCD spectra after heating, in principle they reflected the contribution of intrinsic chiroptical responses of HPNRs (dash curve in figures). Different from the dimeric metamolecules of two identical HPNRs, here the whole chiroptical responses are dominated by the coupling of two nanoparticles. In specific, the left-handed conformations all exhibit a peak-to-trough shape at the long wavelength correlated to the longitudinal coupling, and vice versa, no matter which HPNR is used. However, the intrinsic properties of HPNRs also affect their overall chiroptical responses, especially at the short wavelength range. At this range, no matter left-handed or right-handed metamolecules, the chiroptical responses generally follow the trends of discrete L- or D-HPNRs despite the transverse coupling obviously alters their intensities. It is noted that these metamolecules exhibit more intense PCD than that of HPNRs, as the AuNRs of this size have higher optical density than HPNRs. For comparison, we also recorded the PCD of corresponding metamolecules of two AuNRs (Fig. S8 in the ESM).

3 Conclusions

In summary, we prepared a series of chirally assembled dimeric plasmonic metamolecules using nanorods with intrinsic chirality as building blocks and investigated their chiroptical responses. We categorized these metamolecules into three types. The first type consists of two identical HPNRs in which the chiroptical responses are dominated by the intrinsic chirality of constituent HPNRs along with the longitudinal coupling which alter their PCD spectra mainly at long wavelength. The second type is dimeric metamolecules with two mirrored HPNRs in which the intrinsic chirality is canceled out and both transverse and longitudinal couplings are quite strong. The third type coupling one achiral AuNR and one chiral NR in which the chiroptical responses are mainly determined by the chiral coupling. These results demonstrate that intrinsic chiral plasmonic nanoparticles could be an intriguing building block for assembling chiral plasmonic nanostructures and devices. By further tuning the intrinsic chirality of nanoparticles, selecting combinations of building blocks and controlling their assembled conformations, the PCD spectra at different wavelength ranges could be tailored much more flexibly and simply based on the dimeric metamolecules, which is hardly to be achieved by conventional chiral plasmonic metamolecules of AuNRs.

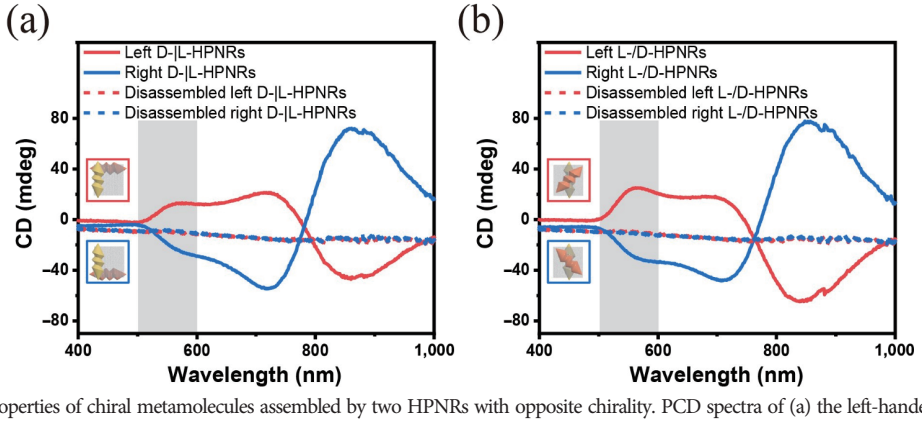

Figure 4 Chiroptical properties of chiral metamolecules assembled by two HPNRs with opposite chirality. PCD spectra of (a) the left-handed (red curve) and right-handed (blue curve) orthogonal dimeric metamolecules; (b) the left-handed (red curve) and right-handed (blue curve) crossed dimeric metamolecules. The dash curves are spectra of respective disassembled metamolecules by heating at 65 °C.

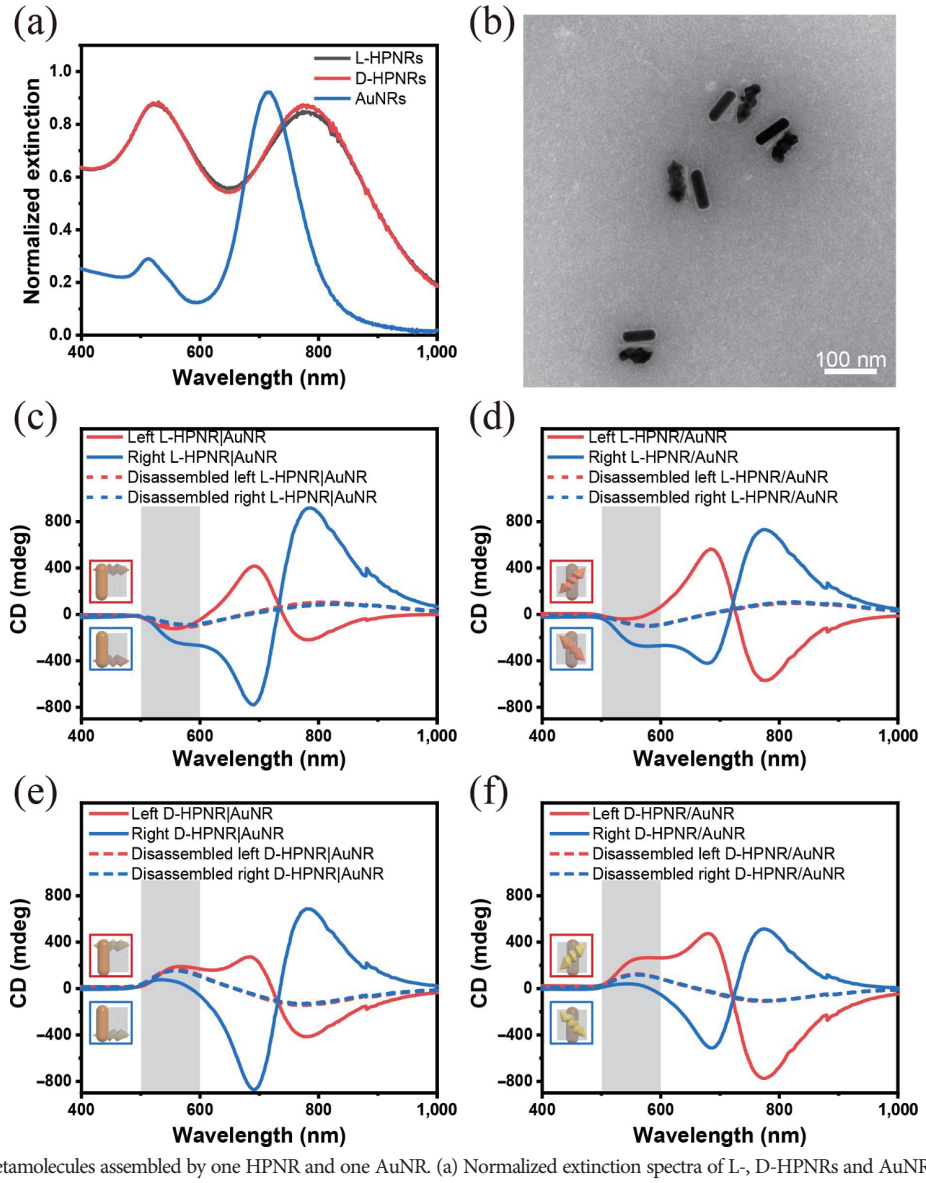

Figure 5 Plasmonic metamolecules assembled by one HPNR and one AuNR. (a) Normalized extinction spectra of L-, D-HPNRs and AuNRs; (b) TEM image of the chiral metamolecules (from metamolecules of right D-HPNR/AuNR). (c)–(f) PCD spectra of the orthogonal and crossed dimeric metamolecules of one L-HPNR and one AuNR ((c) and (d)) and of the orthogonal and crossed dimeric metamolecules of one L-HPNR and one AuNR ((e) and (f)). As above figures, the red curves are left-handed and the blue ones are right-handed; the dash curves are disassembled, respectively.

4 Experimental

4.1 Materials

Gold chloride trihydrate ($HAuCl_4{\cdot}3H_2O$, > 99%) was purchased from Sinopharm Chemical Reagent Co., Ltd. (Shanghai, China). Cetyltrimethylammonium bromide (CTAB, >99%), sodium dodecyl sulfate (SDS), 5-bromosalicylic acid (5-BrSA), 4-aminothiophenol (4-ATP) were obtained from Sigma Aldrich. Sodium borohydride ($NaBH_4$, 99%), silver nitrate ($AgNO_3$), tris(2-carboxyethyl) phosphine (TCEP) were purchased from Acros. L-ascorbic acid (AA), and L- and D-cysteine were purchased from Alfa Aesar. Non-thiolated DNA sequences were bought from Azenta Suzhou, China. Thiolated DNA sequences of HPLC grade were bought from Sangon Biotech (Shanghai) Co., Ltd. The p8064 DNA scaffold DNA was purchased from tilibit nanosystems GmbH (Garching, Germany). All reagents were used as received without further purification. All solutions were prepared using ultrapure water (18.2 MΩ).

4.2 Methods

Synthesis of HPNRs. The AuNRs with average dimensions of 10 nm × 49 nm were synthesized through seed-mediated growth following the reported protocol [48]. The AuNRs solution was centrifuged at a rate of 8,000× g for 15 min and re-dispersed in an aqueous CTAB solution (10 mM) to obtain AuNR/CTAB solution (0.5 nM). To synthesize L-HPNRs (D-HPNRs), the AuNR/CTAB solution was co-incubated with L-cysteine (D- cysteine) and 4-ATP at 30 °C for 3 h. The [cysteine] was 60 μM and [4-ATP] was 40 μM (notably, 4-ATP was dissolved in ethanol). Then $AgNO_3$, $HAuCl_4$, and AA solution were added to the solution one by one. The final concentrations of $AgNO_3$, $HAuCl_4$, and AA were 0.08, 0.12 and 1.64 mM, respectively. After mixed thoroughly, the solution grew in a water bath at 70 °C for 1 h.

DNA modification of HPNRs. Thiolated DNA dissolved in 1× tris-EDTA (TE) buffer was incubated with TCEP for 30 min to reduce the disulfide bonds. The ratio of DNA:TCEP was 1:50. The HPNRs (0.5 nM, 1 mL) synthesized above were centrifuged at 7,000× g and resuspended with 0.5 mL deionized water to remove excess CTAB. Then the solution was concentrated to 10–30 μL by centrifugation. Thiolated DNA strand (500 μM, 8 μL) was incubated with the concentrated solution for 20 min. Then the solution was mixed with 0.5× tris-borate-ethylenediamine tetraacetic acid (TBE) and 0.02% SDS buffer (870 μL) and NaCl

(5 M, 10 μL) was added every 20 min for 10 times. The thiolated DNA modified HPNRs were purified by centrifugation to remove excess free DNA strands before use.

Design, preparation, and purification of two-layer DNA origami. The double-layer square DNA origami templates were designed by CaDNAno [49]. For preparing the DNA origami, 10 nM of the p8064 scaffold, and staple mixture containing 100 nM of each staple type were used. All DNA strands were mixed in deionized water together with 12 mM $MgCl_2$ and 5 mM NaCl in 0.5× TE buffer. The mixture was then annealed as follows: 85 °C for 5 min; from 65 to 61 °C, −1 °C/5 min; from 60 to 51 °C, −1 °C/60 min; from 51 to 38 °C, −1 °C/20 min; from 37 to 26 °C, −1 °C/10 min; held at 25 °C. The origami was then purified by 1% agarose gel electrophoresis in an ice bath using 0.5× TBE-Mg^{2+} as running buffer.

Fabrication and purification of chiral HPNR metamolecules. The thiolated DNA modified HPNRs were mixed with the purified DNA origami at a molar ratio of 5:1, and then annealed as follows: from 35 to 30 °C, −1 °C/3 h; from 30 to 25 °C, −1 °C/2 h; held at 25 °C. The HPNR-origami conjugates were then purified by gel electrophoresis (0.5% agarose) under an ice bath in 0.5× TBE-Mg^{2+} buffer to remove excess HPNRs.

Characterization. The absorption spectra of the DNA origami templates and the HPNRs were measured by using a Thermo Scientific ultraviolet–visible (UV–vis) spectrometer. The concentration of the DNA origami was determined by absorption at 260 nm after purification. The PCD spectra were collected on an Applied Photophysics Chirascan-plus circular dichroism (CD) spectrometer. The measurement was carried out at the wavelength range of 400 nm–1,000 nm at 25 °C in a 10 mm length cell. All the products were diluted by 0.5× TBE-Mg^{2+} buffer. The scanning speed was 100 nm/min. Hitachi HT7700 TEM (100 kV) was used for TEM imaging. The purified samples were dropped on a Glow-discharge grid for 20 s upon staining the samples with 1% uranyl acetate for 20 s. The liquid was removed by filter paper and the grid was left for 30 min to completely dry before injecting into the TEM.

The *g*-factor, also known as the anisotropy factor, was calculated using

$$g = \frac{\text{PCD (in mdeg)}}{33,000 \times \text{absorbance}}$$

Both the PCD and the absorbance were measured simultaneously by the CD spectrometer.

Acknowledgements

This work was financially supported by the National Natural Science Foundation of China (Nos. 21977112, and 21934007), the Natural Science Foundation of Jiangsu Province (No. BK20190227), the Strategic Priority Research Program of Chinese Academy of Sciences (No. XDB36000000) and the Science and Technology Project of Suzhou (No. SZS201904).

Electronic Supplementary Material: Supplementary material (further details of the design of DNA origami, additional agarose gel electrophoresis, TEM images and UV–vis extinction spectra) is available in the online version of this article at https://doi.org/10.1007/s12274-022-4520-2.

References

[1] Willets, K. A.; Van Duyne, R. P. Localized surface plasmon resonance spectroscopy and sensing. *Annu. Rev. Phys. Chem.* **2007**, *58*, 267–297.

[2] Liz-Marzán, L. M. Plasmonics. Electron oscillations and beyond.. *J. Phys. Chem. Lett.* **2013**, *4*, 1197–1198.

[3] Kelly, K. L.; Coronado, E.; Zhao, L. L.; Schatz, G. C. The optical properties of metal nanoparticles: The influence of size, shape, and dielectric environment. *J. Phys. Chem. B* **2003**, *107*, 668–677.

[4] Lee, K. S.; El-Sayed, M. A. Gold and silver nanoparticles in sensing and imaging: Sensitivity of plasmon response to size, shape, and metal composition. *J. Phys. Chem. B* **2006**, *110*, 19220–19225.

[5] Ghosh, S. K.; Pal, T. Interparticle coupling effect on the surface plasmon resonance of gold nanoparticles: From theory to applications. *Chem. Rev.* **2007**, *107*, 4797–4862.

[6] Ding, B. Q.; Deng, Z. T.; Yan, H.; Cabrini, S.; Zuckermann, R. N.; Bokor, J. Gold nanoparticle self-similar chain structure organized by DNA origami. *J. Am. Chem. Soc.* **2010**, *132*, 3248–3249.

[7] Niu, R. J.; Song, C. Y.; Gao, F.; Fang, W. N.; Jiang, X. Y.; Ren, S. K.; Zhu, D.; Su, S.; Chao, J.; Chen, S. F. et al. DNA origami-based nanoprinting for the assembly of plasmonic nanostructures with single-molecule surface-enhanced Raman scattering. *Angew. Chem., Int. Ed.* **2021**, *60*, 11695–11701.

[8] Zhan, P. F.; Wen, T.; Wang, Z. G.; He, Y. B.; Shi, J.; Wang, T.; Liu, X. F.; Lu, G. W.; Ding, B. Q. DNA origami directed assembly of gold bowtie nanoantennas for single-molecule surface-enhanced Raman scattering. *Angew. Chem., Int. Ed.* **2018**, *57*, 2846–2850.

[9] Trofymchuk, K.; Glembockyte, V.; Grabenhorst, L.; Steiner, F.; Vietz, C.; Close, C.; Pfeiffer, M.; Richter, L.; Schütte, M. L.; Selbach, F. et al. Addressable nanoantennas with cleared hotspots for single-molecule detection on a portable smartphone microscope. *Nat. Commun.* **2021**, *12*, 950.

[10] Song, M.; Tong, L. M.; Liu, S. L.; Zhang, Y. W.; Dong, J. Y.; Ji, Y. L.; Guo, Y.; Wu, X. C.; Zhang, X. D.; Wang, R. Y. Nonlinear amplification of chirality in self-assembled plasmonic nanostructures. *ACS Nano* **2021**, *15*, 5715–5724.

[11] Wang, Z. Y.; Zhang, N. N.; Li, J. C.; Lu, J.; Zhao, L.; Fang, X. D.; Liu, K. Serum albumin guided plasmonic nanoassemblies with opposite chiralities. *Soft Matter* **2021**, *17*, 6298–6304.

[12] Han, B.; Shi, L.; Gao, X. Q.; Guo, J.; Hou, K.; Zheng, Y. L.; Tang, Z. Y. Ultra-stable silica-coated chiral au-nanorod assemblies: Core-shell nanostructures with enhanced chiroptical properties. *Nano Res.* **2016**, *9*, 451–457.

[13] Fan, Z. Y.; Govorov, A. O. Helical metal nanoparticle assemblies with defects: Plasmonic chirality and circular dichroism. *J. Phys. Chem. C* **2011**, *115*, 13254–13261.

[14] Auguié, B.; Alonso-Gómez, J. L.; Guerrero-Martínez, A.; Liz-Marzán, L. M. Fingers crossed: Optical activity of a chiral dimer of plasmonic nanorods. *J. Phys. Chem. Lett.* **2011**, *2*, 846–851.

[15] Lu, J.; Xue, Y.; Bernardino, K.; Zhang, N. N.; Gomes, W. R.; Ramesar, N. S.; Liu, S. H.; Hu, Z.; Sun, T. M.; De Moura, A. F. et al. Enhanced optical asymmetry in supramolecular chiroplasmonic assemblies with long-range order. *Science* **2021**, *371*, 1368–1374.

[16] Pal, S.; Deng, Z. T.; Wang, H. N.; Zou, S. L.; Liu, Y.; Yan, H. DNA directed self-assembly of anisotropic plasmonic nanostructures. *J. Am. Chem. Soc.* **2011**, *133*, 17606–17609.

[17] Liu, W. Y.; Halverson, J.; Tian, Y.; Tkachenko, A. V.; Gang, O. Self-organized architectures from assorted DNA-framed nanoparticles. *Nat. Chem.* **2016**, *8*, 867–873.

[18] Zhao, Z.; Chen, X. H.; Zuo, J. W.; Basiri, A.; Choi, S.; Yao, Y.; Liu, Y.; Wang, C. Deterministic assembly of single emitters in sub-5 nanometer optical cavity formed by gold nanorod dimers on three-dimensional DNA origami. *Nano Res.* **2022**, *15*, 1327–1337.

[19] Kuzyk, A.; Jungmann, R.; Acuna, G. P.; Liu, N. DNA origami route for nanophotonics. *ACS Photonics* **2018**, *5*, 1151–1163.

[20] Liu, S. B.; Shang, Y. X.; Jiao, Y. F.; Li, N.; Ding, B. Q. DNA-based plasmonic nanostructures and their optical and biomedical applications. *Nanotechnology* **2021**, *32*, 402002.

[21] Kuzyk, A.; Schreiber, R.; Fan, Z. Y.; Pardatscher, G.; Roller, E. M.; Högele, A.; Simmel, F. C.; Govorov, A. O.; Liedl, T. DNA-based self-assembly of chiral plasmonic nanostructures with tailored optical response. *Nature* **2012**, *483*, 311–314.

[22] Shen, X. B.; Song, C.; Wang, J. Y.; Shi, D. W.; Wang, Z. A.; Liu, N.; Ding, B. Q. Rolling up gold nanoparticle-dressed DNA origami

into three-dimensional plasmonic chiral nanostructures. *J. Am. Chem. Soc.* **2012**, *134*, 146–149.

[23] Shen, X. B.; Asenjo-Garcia, A.; Liu, Q.; Jiang, Q.; de Abajo, F. J. G.; Liu, N.; Ding, B. Q. Three-dimensional plasmonic chiral tetramers assembled by DNA origami. *Nano Lett.* **2013**, *13*, 2128–2133.

[24] Shen, X. B.; Zhan, P. F.; Kuzyk, A.; Liu, Q.; Asenjo-Garcia, A.; Zhang, H.; de Abajo, F. J. G.; Govorov, A.; Ding, B. Q.; Liu, N. 3D plasmonic chiral colloids. *Nanoscale* **2014**, *6*, 2077–2081.

[25] Lan, X.; Lu, X. X.; Shen, C. Q.; Ke, Y. G.; Ni, W. H.; Wang, Q. B. Au nanorod helical superstructures with designed chirality. *J. Am. Chem. Soc.* **2015**, *137*, 457–462.

[26] Liu, Y.; Ma, L.; Jiang, S. X.; Han, C.; Tang, P.; Yang, H.; Duan, X. Y.; Liu, N.; Yan, H.; Lan, X. DNA programmable self-assembly of planar, thin-layered chiral nanoparticle superstructures with complex two-dimensional patterns. *ACS Nano* **2021**, *15*, 16664–16672.

[27] Kuzyk, A.; Schreiber, R.; Zhang, H.; Govorov, A. O.; Liedl, T.; Liu, N. Reconfigurable 3D plasmonic metamolecules. *Nat. Mater.* **2014**, *13*, 862–866.

[28] Zhou, C.; Duan, X. Y.; Liu, N. A plasmonic nanorod that walks on DNA origami. *Nat. Commun.* **2015**, *6*, 8102.

[29] Xin, L.; Zhou, C.; Duan, X. Y.; Liu, N. A rotary plasmonic nanoclock. *Nat. Commun.* **2019**, *10*, 5394.

[30] Dong, J. Y.; Wang, M.; Zhou, Y. H.; Zhou, C.; Wang, Q. B. DNA-based adaptive plasmonic logic gates. *Angew, Chem., Int. Ed.* **2020**, *59*, 15038–15042.

[31] Hentschel, M.; Schäferling, M.; Duan, X. Y.; Giessen, H.; Liu, N. Chiral plasmonics. *Sci. Adv.* **2017**, *3*, e1602735.

[32] Klös, G.; Andersen, A.; Miola, M.; Birkedal, H.; Sutherland, D. S. Oxidation controlled lift-off of 3D chiral plasmonic Au nano-hooks. *Nano Res.* **2019**, *12*, 1635–1642.

[33] Kim, J. Y.; Yeom, J.; Zhao, G. P.; Calcaterra, H.; Munn, J.; Zhang, P. J.; Kotov, N. Assembly of gold nanoparticles into chiral superstructures driven by circularly polarized light. *J. Am. Chem. Soc.* **2019**, *141*, 11739–11744.

[34] Lee, H. E.; Ahn, H. Y.; Mun, J.; Lee, Y. Y.; Kim, M.; Cho, N. H.; Chang, K.; Kim, W. S.; Rho, J.; Nam, K. T. Amino-acid-and peptide-directed synthesis of chiral plasmonic gold nanoparticles. *Nature* **2018**, *556*, 360–365.

[35] Cho, N. H.; Byun, G. H.; Lim, Y. C.; Im, S. W.; Kim, H.; Lee, H. E.; Ahn, H. Y.; Nam, K. T. Uniform chiral gap synthesis for high dissymmetry factor in single plasmonic gold nanoparticle. *ACS Nano* **2020**, *14*, 3595–3602.

[36] Lee, H. E.; Kim, R. M.; Ahn, H. Y.; Lee, Y. Y.; Byun, G. H.; Im, S. W.; Mun, J.; Rho, J.; Nam, K. T. Cysteine-encoded chirality evolution in plasmonic rhombic dodecahedral gold nanoparticles. *Nat. Commun.* **2020**, *11*, 263.

[37] González-Rubio, G.; Mosquera, J.; Kumar, V.; Pedrazo-Tardajos, A.; Llombart, P.; Solís, D. M.; Lobato, I.; Noya, E. G.; Guerrero-Martínez, A.; Taboada, J. M. et al. Micelle-directed chiral seeded growth on anisotropic gold nanocrystals. *Science* **2020**, *368*, 1472–1477.

[38] Wang, S.; Zheng, L. H.; Chen, W. J.; Ji, L. K.; Zhang, L.; Lu, W. S.; Fang, Z. Y.; Guo, F. C.; Qi, L. M.; Liu, M. H. Helically grooved gold nanoarrows: Controlled fabrication, superhelix, and transcribed chiroptical switching. *CCS Chemistry* **2021**, *3*, 2473–2484.

[39] Chen, J. Q.; Gao, X. S.; Zheng, Q.; Liu, J. B.; Meng, D. J.; Li, H. Y.; Cai, R.; Fan, H. Z.; Ji, Y. L.; Wu, X. C. Bottom-up synthesis of helical plasmonic nanorods and their application in generating circularly polarized luminescence. *ACS Nano* **2021**, *15*, 15114–15122.

[40] Xu, L. G.; Wang, X. X.; Wang, W. W.; Sun, M. Z.; Choi, W. J.; Kim, J. Y.; Hao, C. L.; Li, S.; Qu, A. H.; Lu, M. R. et al. Enantiomer-dependent immunological response to chiral nanoparticles. *Nature* **2022**, *601*, 366–373.

[41] Zhang, N. N.; Sun, H. R.; Liu, S. H.; Xing, Y. C.; Lu, J.; Peng, F.; Han, C. L.; Wei, Z. L.; Sun, T. M.; Yang, B. et al. Gold nanoparticle enantiomers and their chiral-morphology dependence of cellular uptake. *CCS Chem.* **2022**, *4*, 660–670.

[42] Zheng, G. C.; Jiao, S. L.; Zhang, W.; Wang, S. L.; Zhang, Q. H.; Gu, L.; Ye, W. X.; Li, J. J.; Ren, X. C ; Zhang, Z. C. et al. Fine-tune chiroptical activity in discrete chiral Au nanorods. *Nano Res.*, in press, https://doi.org/10.1007/s12274-022-4212-y.

[43] Zheng, G. C.; Bao, Z. Y.; Pérez-Juste, J.; Du, R. L.; Liu, W.; Dai, J. Y.; Zhang, W.; Lee, L. Y. S.; Wong, K. Y. Tuning the morphology and chiroptical properties of discrete gold nanorods with amino acids. *Angew. Chem., Int. Ed.* **2018**, *57*, 16452–16457.

[44] Hao, C. L.; Xu, L. G.; Sun, M. Z.; Ma, W.; Kuang, H.; Xu, C. L. Chirality on hierarchical self-assembly of Au@AuAg yolk-shell nanorods into core-satellite superstructures for biosensing in human cells. *Adv. Funct. Mater.* **2018**, *28*, 1802372.

[45] Zheng, G. C.; He, J. J.; Kumar, V.; Wang, S. L.; Pastoriza-Santos, I.; Pérez-Juste, J.; Liz-Marzán, L. M.; Wong, K. Y. Discrete metal nanoparticles with plasmonic chirality. *Chem. Soc. Rev.* **2021**, *50*, 3738–3754.

[46] Dong, J. Y.; Zhou, Y. H.; Pan, J. H.; Zhou, C.; Wang, Q. B. Assembling gold nanobipyramids into chiral plasmonic nanostructures with DNA origami. *Chem. Commun.* **2021**, *57*, 6201–6204.

[47] Fan, Z. Y.; Govorov, A. O. Chiral nanocrystals: Plasmonic spectra and circular dichroism. *Nano Lett.* **2012**, *12*, 3283–3289.

[48] Ye, X. C.; Jin, L. H.; Caglayan, H.; Chen, J.; Xing, G. Z.; Zheng, C.; Doan-Nguyen, V.; Kang, Y. J.; Engheta, N.; Kagan, C. R. et al. Improved size-tunable synthesis of monodisperse gold nanorods through the use of aromatic additives. *ACS Nano* **2012**, *6*, 2804–2817.

[49] Douglas, S. M.; Marblestone, A. H.; Teerapittayanon, S.; Vazquez, A.; Church, G. M.; Shih, W. M. Rapid prototyping of 3D DNA-origami shapes with caDNAno. *Nucleic Acids Res.* **2009**, *37*, 5001–5006.